Atmospheric Environment 151 (2017) 24–33

Contents lists available at ScienceDirect

Atmospheric Environment

journal homepage: www.elsevier.com/locate/atmosenv

Trend analysis of CO_2 and CH_4 recorded at a semi-natural site in the northern plateau of the Iberian Peninsula

Isidro A. Pérez*, M. Luisa Sánchez, M. Ángeles García, Nuria Pardo

Department of Applied Physics, Faculty of Sciences, University of Valladolid, Paseo de Belén, 7, 47011 Valladolid, Spain

HIGHLIGHTS

- Four procedures were used to obtain the CO_2 and CH_4 trend and seasonal behaviour.
- A time-dependent amplitude was considered in the harmonic equation.
- Similar trends were obtained with the methods employed.
- Kernel regression stands out among the nonparametric procedures used.

ARTICLE INFO

Article history:
Received 30 June 2016
Received in revised form
28 November 2016
Accepted 29 November 2016
Available online 30 November 2016

Keywords:
Carbon dioxide
Methane
Long-term analysis
Kernel smoothing
Local regression

ABSTRACT

CO_2 and CH_4 were recorded from October 2010 to February 2016 with a Picarro G1301 analyser at the centre of the upper plateau of the Iberian Peninsula. Large CO_2 values were observed during the vegetation growing season, and were reinforced by the stable boundary layer during the night. Annual CH_4 evolution may be explained by ecosystem activity and by the dispersion linked with the evolution of the boundary layer. Their trends were studied using an equation that considers one polynomial and one harmonic part. The polynomial part revealed an increasing trend from 0.8 to 2.3 ppm year^{-1} for CO_2 and from 0.004 to 0.011 ppm year^{-1} for CH_4. The harmonic part considered four harmonics whose amplitudes were noticeable for the first and second harmonics for CO_2 and for the first harmonic for CH_4. Long-term evolution was similar with alternative equations. Finally, seasonal study indicated summer minima for both gases, which may be explained by the lack of vegetation in this season. Harmonic analysis showed two maxima for CO_2, one in spring linked with vegetation growth, which decreased with time, and another in autumn related with the onset of plant activity after the summer, which increased with time. CH_4 presented only one maximum in winter and a short time with steady concentration in spring where the evolution of the boundary layer may play a noticeable role. The harmonic equation, which takes into account all the observations, revealed opposite behaviour between CO_2, whose minima decreased, and CH_4, whose maxima increased.

1. Introduction

CO_2 and CH_4 are trace gases involved in the greenhouse effect whose observations are continuously recorded worldwide (NOAA, 2016; WDCGG, 2016). Mauna Loa was the site where continuous measurements of atmospheric CO_2 commenced in 1958. Since this year, the number of observatories has increased considerably. In particular, measurements started at certain stations during the nineties. In Europe, Vermeulen et al. (2011) have presented measurements since 1993 at Cabauw in the Netherlands, and Lohila et al. (2015) indicated that CO_2 has been measured since 1998 and CH_4 since 2004 at Sammaltunturi, Finland. In North America, CO_2 observations commenced in 1990 at the top of a 40-m tower at Fraserdale, Canada (Higuchi et al., 2003). This trace gas has been measured since 1992 on a 610-m tower in North Carolina and since 1994 on a 447-m tower in Wisconsin (Bakwin et al., 1998). In Asia, Inoue et al. (2006) considered CO_2 recordings from a 200-m tower at Tsukuba, Japan, from 1992. At Minamitorishima station, western North Pacific, these trace gases have been measured since 1993 (Wada et al., 2007), and CH_4 measurements began at Waliguan, China, in 1994 (Zhang et al., 2013).

CO_2 natural sources are respiration processes and main

* Corresponding author.
E-mail address: iaperez@fa1.uva.es (I.A. Pérez).

http://dx.doi.org/10.1016/j.atmosenv.2016.11.068
1352-2310/

anthropogenic sources are combustion of fossil fuels. The global anthropogenic emissions inventory of gaseous and particulate air pollutants, EDGAR, published by the European Commission revealed that the greatest emissions corresponded to China and the USA in 2014. Moreover, the increase in these global emissions almost stalled in that year. Specifically, they decreased from 4.1 to 3.4 billion tonnes between 2000 and 2014 in the European Union (Olivier et al., 2015). Natural sinks are the uptake by oceans and photosynthesis. As a result, CO_2 atmospheric lifetime is 30–95 years (Jacobson, 2005). Its distribution over the globe presented concentrations around 400 ppm in the northern hemisphere in 2015, whereas they were slightly lower than this value in the southern hemisphere. Average seasonal evolution showed an accentuated cycle in the northern hemisphere with a maximum in winter-spring and a minimum in August–September. Tropospheric CO_2 is increasing, its rate depending on ecosystem evolution and measurement time, since observations indicate an irregular increase following the background concentration evolution (WMO, 2016). Hence, accurate determination of the CO_2 trend should be obtained, since this also plays a useful role in investigating whether the control strategies for this gas's emissions are correct.

Initially, the current analysis takes an expression formed by one polynomial and one harmonic part, the first for the trend and the second part for seasonal behaviour. A specific part of this study is devoted to analysing the harmonic part. Although such an expression is frequently used, its detailed analysis is usually limited to amplitude, which is assumed constant in most of the research undertaken to date (Timokhina et al., 2015). The inclusion of time in the amplitude of the harmonic function is a major contribution made by the present research and provides a more in-depth analysis of seasonal evolution.

Moreover, alternative procedures such as kernel regression, weighted linear regression and weighted quadratic regression are applied to investigate not only the long-term evolution but also the seasonal cycle, with their features, advantages, and drawbacks being discussed and compared.

CH_4 is another greenhouse gas whose behaviour has been less widely studied to date. Anthropogenic sources are biomass burning, landfills, crops such as rice paddies and fossil fuel production and consumption. Natural sources are wetlands, oceans, geological seeps or enteric fermentation. Its main sink is oxidation by the hydroxyl radical (OH) in the troposphere, which means a lifetime of about 10 years. Its evolution over the globe may be observed from WMO (2016). In 2015, its concentration was above 1.9 ppm for latitudes higher than 30° N, whereas it was below 1.8 ppm in the southern hemisphere. Seasonal evolution was slightly more accentuated in the Northern Hemisphere, where the maximum was reached in winter and the minimum in summer. Recently, Sánchez et al. (2014) investigated its directional behaviour as well as daily and yearly cycles in the upper Spanish plateau, and García et al. (2016) considered the influence of atmospheric stability and transport on its concentrations at the same site. In the current research, CH_4 analysis will run parallel to that of CO_2.

2. Materials and methods

2.1. Experimental description

CO_2 and CH_4 dry concentrations were measured with a Picarro G1301 at CIBA (Low Atmosphere Research Centre) 41° 48′ 50.27″ N, 4° 55′ 58.44″ W, at 852 m above mean sea level. The measurements considered in this paper began on 15 October 2010 and extended to 29 February 2016. The analyser uses the wavelength-scanned cavity ringdown spectroscopy technique (Crosson, 2008) and achieves the WMO inter-laboratory comparability standard for both gases without drying the sample gas (Chen et al., 2010; Rella, 2010; Rella et al., 2013). It was equipped with a valve sequencer to obtain observations at 1.8, 3.7 and 8.3 m every 10 min at each level. Around 30 observations were taken each minute, although values were averaged every half an hour. Calibrations made every two weeks with three NOAA standards revealed the extreme stability of the device and were used to slightly correct observations applying the following linear equations (in ppm):

$$CO_{2\,C} = 1.00341\ CO_2 - 0.17870 \tag{1}$$

$$CH_{4\,C} = 0.99197\ CH_4 + 0.01249 \tag{2}$$

where the C subscript denotes the corrected value.

2.2. Harmonic regression

The CO_2 time series may be considered to comprise three components, the trend component, the seasonal component and the remainder component (Cleveland et al., 1990). One initial problem concerns the separation between the seasonal cycle and the long-term evolution. Thoning and Tans (1989) introduced a digital filtering technique to achieve this objective. However, simpler alternative procedures have successfully been considered. At Lampedusa, Artuso et al. (2009) used an exponential function to describe the long-term CO_2 trend whose fit is not possible by linear regression. Measurements reveal that this trend is not affected by sharp changes and may be approximated by a linear term (Chamard et al., 2003), which is usually extended to a polynomial equation.

The current analysis is based on the procedure presented by Nakazawa et al. (1997), which used an equation with polynomial and harmonic parts similar to

$$y = \sum_{i=0}^{3} a_i t^i + \sum_{j=1}^{4} \sum_{k=0}^{1} \left(b_{jk} \mathrm{t}^{\mathrm{k}} \cos(j2\pi t) + c_{jk} \mathrm{t}^{\mathrm{k}} \sin(j2\pi t) \right) \tag{3}$$

This equation is taken as a reference since it has often been used in similar studies, such as Bakwin et al. (1998) or Fang et al. (2016). Eneroth et al. (2005) and Inoue et al. (2006) used equations with three harmonics. However, this paper considers four harmonics, in agreement with Tans et al. (1989) and Vermeulen et al. (2011), although both analyses evidence a linear trend. However, the main contribution of equation (3) is the time affecting the amplitude. In our case, y is CO_2 or CH_4 concentrations and t is the time measured in years.

Equation (3) is proposed to describe the global evolution by the polynomial part and the evolution of the yearly cycle by the harmonic part. First and second harmonics are related with the yearly cycle, since the first harmonic proposes times and values for the yearly maxima and minima and the second corrects or reinforces them. However, the remaining harmonics considered focus on the seasonal pattern. Consequently, shorter time intervals are not taken into account by Eq. (3).

In the case of a slow time variation in the amplitude of each frequency, Eq. (3) may be written as

$$y = \sum_{i=0}^{3} a_i t^i + \sum_{j=1}^{4} \mathrm{A_j(t)} \cos\left(\frac{2\pi t}{T_j} - \theta_j \right) \tag{4}$$

where amplitude $A_j(t)$, period T_j and phase constant θ_j must be determined experimentally. For each frequency j of Eq. (3), the N maxima of the harmonic part are determined, $Y_{j1} \ldots Y_{jN}$. The time between consecutive maxima, t_{ji+1}-t_{ji}, is one period, resulting in N-1 periods. The average period, T_j, may be calculated. Since the phase

must be null for every maximum of Eq. (4), the phase constant, θ_{ji}, may be obtained from each time t_{ji} corresponding to maxima Y_{ji}. In order to avoid the discontinuity of this angular variable at 0°, θ_{ji} should be treated as a vector and its components, cos θ_{ji} and sin θ_{ji}, should be calculated and averaged to obtain the mean phase constant, θ_j.

Finally, amplitude is calculated by linear interpolations between consecutive maxima and extrapolations at the edges, before the first maximum and beyond the last maximum.

$$A_j(t) = \begin{cases} Y_{j1} + \dfrac{Y_{j2} - Y_{j1}}{t_{j2} - t_{j1}}(t - t_{j1}) \text{ if } t < t_{j1} \\ Y_{ji} + \dfrac{Y_{ji+1} - Y_{ji}}{t_{ji+1} - t_{ji}}(t - t_{ji}) \text{ if } t_{ji} < t < t_{ji+1} \\ Y_{jN-1} + \dfrac{Y_{jN} - Y_{jN-1}}{t_{jN} - t_{jN-1}}(t - t_{jN-1}) \text{ if } t_{jN} < t \end{cases} \quad (5)$$

2.3. Kernel regression

This is a weighted mean calculated by

$$y(t,h) = \frac{\sum_{i=1}^{N} K\left(\frac{t-t_i}{h}\right) y_i}{\sum_{i=1}^{N} \left(\frac{t-t_i}{h}\right)} \quad (6)$$

where t is the time when the concentration y is calculated, y_i are experimental values of concentration at t_i, h is the width of a window and K is the kernel function. The Gaussian kernel has sometimes been used (Donnelly et al., 2011), since it includes all observations. However, the extremely long time required to make the calculations when many observations are involved has led to it being replaced by the Epanechnikov kernel,

$$K\left(\frac{t-t_i}{h}\right) = 0.75\left(1 - \left(\frac{t-t_i}{h}\right)^2\right), \; -1 \le \frac{t-t_i}{h} \le 1 \quad (7)$$

which was also used in this kind of calculations (Henry et al., 2002). Only observations t_i ranging from t-h to $t + $ h are considered in this kernel.

The procedure followed in this paper was based on Graven et al. (2012). Observations were first detrended with a wide window, and seasonal cycles were considered by smoothing the detrended observations with a narrow window. Finally, these seasonal cycles were subtracted from the original observations and the resulting series was smoothed again with the initial window. The narrow window was 60 days so as to consider seasonal changes, whereas a test was conducted to choose the wide window with values from 300 to 1000 days in 100-day intervals. Oscillations disappeared with a 500-day window, which was the value selected.

A noticeable feature of this procedure is that only half the observations take part in calculations at the beginning or end of the measurement period.

2.4. Other nonparametric procedures

Some local regression methods were suggested by Cleveland (1979) and Cleveland and Devlin (1988) to obtain visual information from a scatterplot.

The tri-cube weight function is usually employed. However, weights are calculated in this paper employing the Epanechnikov kernel to use the same weight function in the procedures presented. Two methods were followed: the first considers a weighted linear regression, $y = a_0 + a_1 t$, whose coefficients were easily calculated by

$$a_1 = \frac{\sum_{i=1}^{q} w_i \left(t_i - \overline{t_w}\right)\left(y_i - \overline{y_w}\right)}{\sum_{i=1}^{q} w_i \left(t_i - \overline{t_w}\right)^2} \quad (8)$$

$$a_0 = \overline{y_w} - a_1 \overline{t_w} \quad (9)$$

where w_i are the weights and $\overline{t_w}$ and $\overline{y_w}$ are obtained from

$$\overline{t_w} = \frac{\sum_{i=1}^{q} w_i t_i}{\sum_{i=1}^{q} w_i} \quad (10)$$

$$\overline{y_w} = \frac{\sum_{i=1}^{q} w_i y_i}{\sum_{i=1}^{q} w_i} \quad (11)$$

and the second used a weighted quadratic regression, $y = b_0 + b_1 t + b_2 t^2$. The coefficient calculation is given by

$$\mathbf{b} = \left(\mathbf{X^T W X}\right)^{-1} \mathbf{X^T W y} \quad (12)$$

where $\mathbf{y}$ is the matrix of the response variable, which is the observed concentration, $\mathbf{W}$ is the diagonal matrix containing the weights, and the matrices $\mathbf{X}$ and $\mathbf{b}$ are

$$\mathbf{X} = \begin{pmatrix} 1 & t_1 & t_1^2 \\ 1 & t_2 & t_2^2 \\ \cdots & \cdots & \cdots \\ 1 & t_n & t_n^2 \end{pmatrix}; \mathbf{b} = \begin{pmatrix} b_0 \\ b_1 \\ b_2 \end{pmatrix} \quad (13)$$

3. Results

Calculations for the harmonic model were made in Matlab since this easily handles multiple linear regressions in addition to which the time employed was short. Its main advantage is that trend calculation and seasonal behaviour analysis are carried out in a single step. The remaining calculations were made in Fortran, with the calculation time being noticeably long for the weighted quadratic regression.

3.1. CO_2 and CH_4 variation

Availability of observations was around 84% due to noticeable gaps in August 2013 and 2015, and from August to the end of 2014. CO_2 median concentration was 401.5 ppm for the 1.8-m level, with an interquartile range of 11.9 ppm. For the 8.3-m level, concentration was 0.6 ppm lower and the interquartile range 1.6 ppm narrower. Observations for the lowest level are presented in Fig. 1 (a) where the seasonal pattern is revealed by noticeable values in spring and low values in summer. Large measurements could be explained by plant respiration during the growing season together with the formation of a stable boundary layer during the night. Occasional emissions from vehicles used in farming around the site should not be excluded. However, the low values observed in summer may be attributed to the lack of vegetation in this season.

For CH_4, median concentration was 1.899 ppm at the lowest level, with an interquartile range of 0.040 ppm, whereas concentration was 0.001 ppm higher with similar interquartile range for

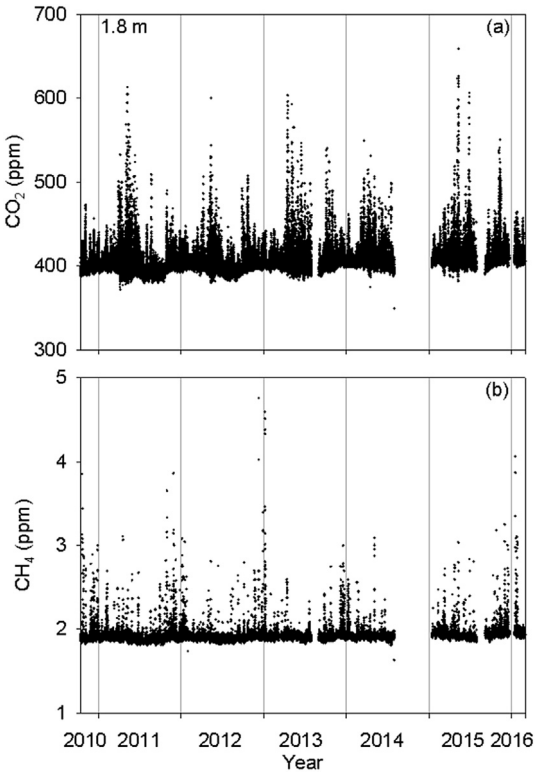

Fig. 1. Observations (half hour averages) for the lowest level considered in the current analysis.

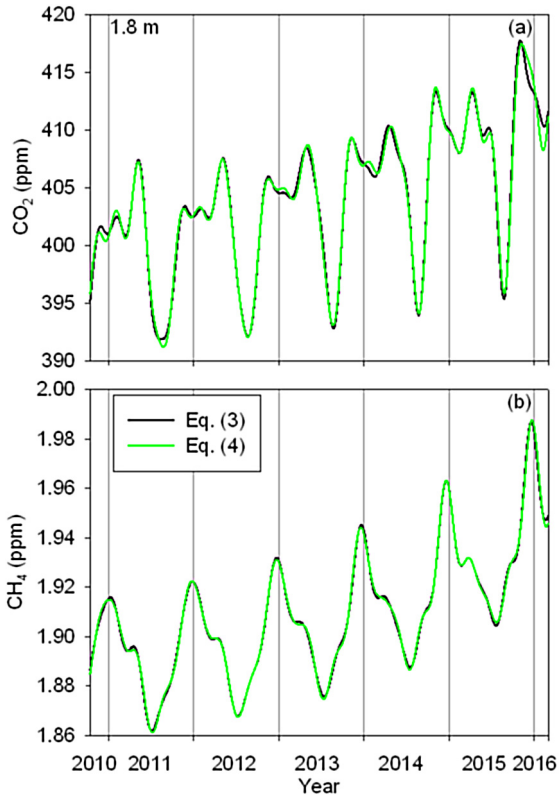

Fig. 2. Evolution for CO_2 (a) and CH_4 (b) obtained with Eqs. (3) and (4), which are formed by a polynomial part and a harmonic part.

the highest level. Its seasonal cycle is much less marked since measurements are located in a very narrow interval, Fig. 1 (b). The largest values were recorded in winter when soil and plant activities increase due to the rains and the low values of the boundary layer height are also reached.

3.2. Harmonic regression

Fig. 2 presents the results of Eqs. (3)–(4) for the lowest level, since the changes are more pronounced for CO_2 than in the other levels. Both gases present an increasing trend with rapid growth over the latter years. The main advantage of this procedure is that the lack of data does not prevent calculations from continuing since this method fills in the gaps.

Following those equations, the CO_2 yearly cycle is described by a maximum in spring linked with the development of vegetation activity, which was noticeable in 2011 but moderate in 2015. A second maximum was observed in autumn, which was attributed to soil and plant activities with the first rains after summer. The contribution of this maximum was slight in 2011, but gradually increased and was noticeable in 2015. The CO_2 minimum was reached in summer, when vegetation almost vanishes. Concentration at this time also increased from 2011 to 2015, although the CO_2 hole was deeper in 2015 than in 2011.

The CH_4 yearly cycle was simpler than that for CO_2. Maxima were observed in winter, whereas minima were found in summer. Moreover, a short period with a steady concentration was observed in spring. In agreement with CO_2, the increase was faster at the end than at the beginning of the period analysed.

Agreement of Eq. (3) was described by R^2, which was between 0.14 and 0.28 for CO_2 at the lowest and highest levels, respectively, and around 0.10 for CH_4. These low values are attributed to the noticeable daily changes of the half hour means that were used. When daily means are considered, values are steadier and R^2 increases, extending from 0.40 to 0.59 for CO_2, whereas it remained around 0.30 for CH_4. Finally, when monthly means are used, R^2 ranged from 0.87 to 0.93 for CO_2 and was around 0.89 for CH_4. Moreover, Fig. (2) shows the satisfactory agreement between Eqs. (3) and (4).

Fig. 3 shows the four harmonics calculated with Eqs. (3) and (4). Two amplitude groups may be observed. For CO_2, the first group is formed by the first and second harmonics, whose greatest amplitudes were slightly below 6 ppm. The second group comprises the third and fourth harmonics, with amplitudes reaching around 3 ppm. For CH_4, the first group is formed by the first harmonic, whose amplitude was around 0.025 ppm, whereas the remaining harmonics make up a second group whose amplitude is around 0.008 ppm at most.

The first harmonic amplitude decreased slightly with time for CO_2, and increased for the CO_2 second harmonic and from the first to third harmonics of CH_4. In these cases, Eq. (5) may be simplified by a linear relationship. The remaining harmonics displayed a more complex evolution with a decreasing trend in the amplitude at the beginning of the period considered and an increasing trend at the end, reaching a minimum in 2012. The contribution of the first harmonic is almost time independent for both trace gases, whereas the fourth harmonic was noticeably small for CH_4 in 2012.

Fig. 3 reveals that the addition of two harmonic functions, one with constant amplitude and the second whose amplitude changes slowly with time, results in a harmonic function whose amplitude changes slowly with time: hence the satisfactory agreement between the harmonic parts of Eqs. (3) and (4).

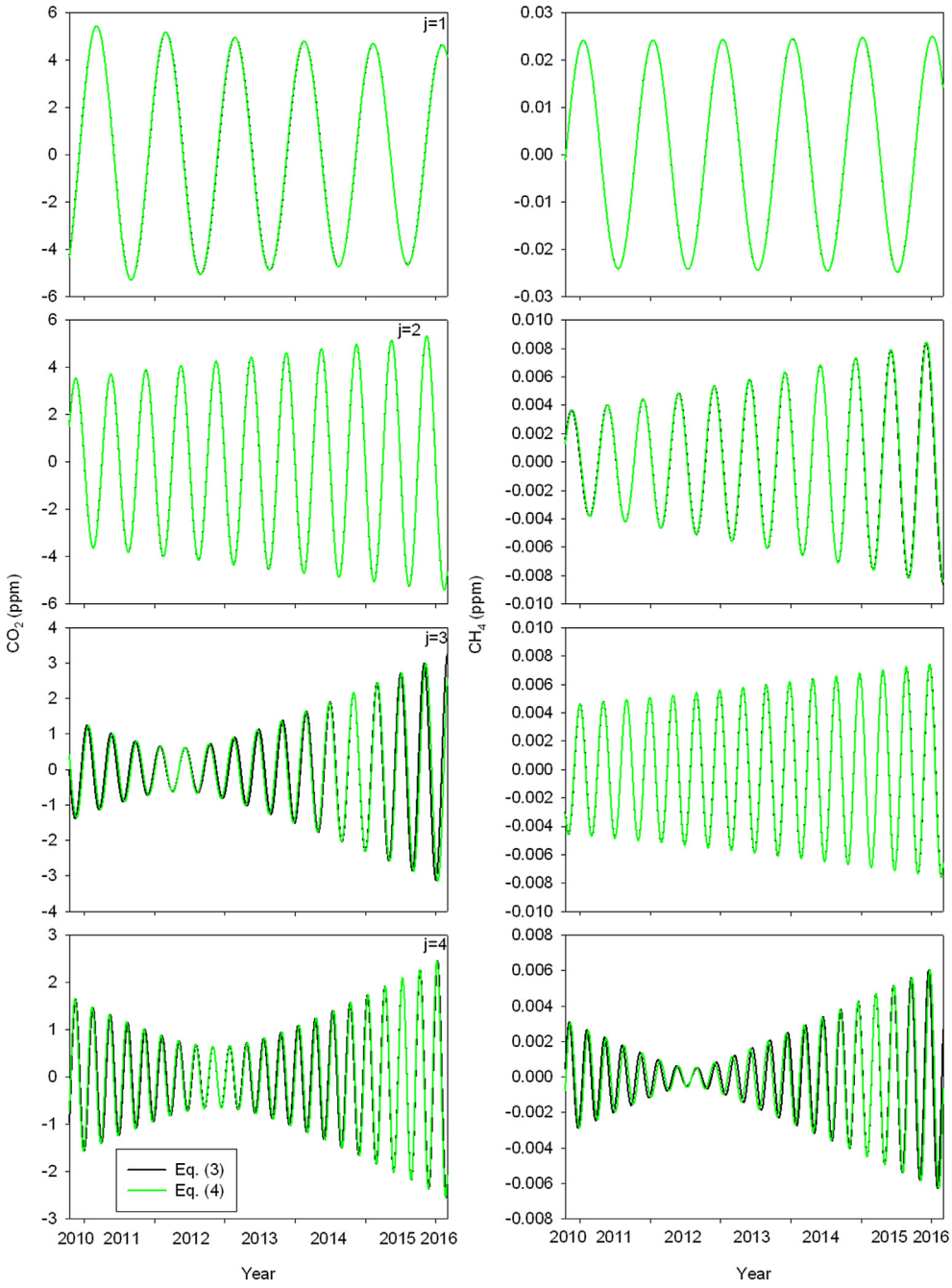

Fig. 3. CO_2 and CH_4 concentrations calculated by the four harmonics used in Eqs. (3) and (4).

3.3. Trend analysis

Fig. 4 presents the evolutions of both trace gases together with their growth rate. CO_2 concentration increased 12.3 ppm during the measurement period for the polynomial part that reveals the trend in Eq. (3). The trend average value was 1.7 ppm year^{-1}. However, this increase was not regular since at the end of 2010 the growth rate was low, around 0.8 ppm year^{-1} whilst, contrastingly, the trend reached 2.3 ppm year^{-1} in early 2016.

For CH_4, the increase was 0.059 ppm, with an average of 0.006 ppm year^{-1}. Its growth rate began at nearly 0.004 ppm year^{-1} and finished at 0.011 ppm year^{-1}. This polynomial evolution was considered a reference since equations similar to Eq. (3) are frequently used.

Alternative procedures showed a similar evolution. The polynomial model determined the steadiest trend. However, small oscillations were observed when the weighted quadratic regression was used. The greatest discrepancies for CH_4 observed at the beginning and end of the measurement period for this latter method could be attributed to a border effect, since calculations were made with half the observations in the window. The fluctuating behaviour of the weighted quadratic regression was noticeable in the growth rate displayed in the lower plots of this figure and is due to the width of the wide window used, i.e. 500 days, which was considered to compare the procedures in similar conditions. When using a wider window, such as 1000 days,

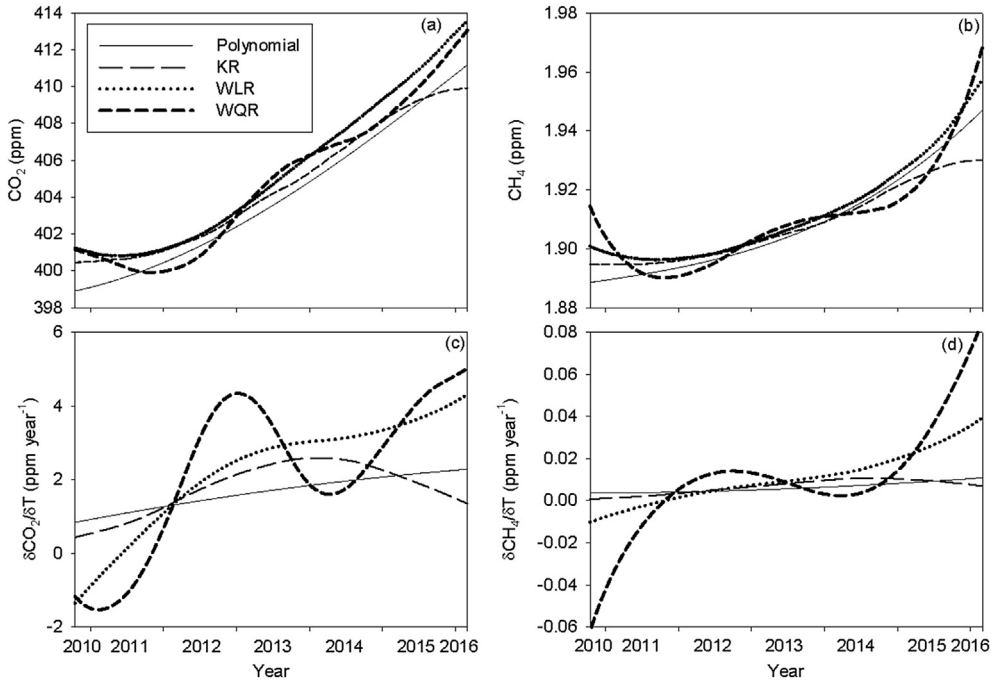

Fig. 4. Trends of CO_2 (a) and CH_4 (b) together with their corresponding growth rates, (c) and (d), for polynomial, kernel regression (KR), weighted linear regression (WLR) and weighted quadratic regression (WQR).

oscillations disappear.

Fig. 5 shows the seasonal evolution formed by the harmonic part of Eq. (3) and once the observations were detrended in the other methods. Spring and autumn CO_2 maxima were noticeable in the harmonic equation. However, the summer CO_2 minima decreased markedly with time despite the lack of observations in August from 2013 to 2015. Moreover, winter CH_4 maxima increased with time.

Seasonal evolution for the kernel regression and weighted linear regression were very similar and revealed noticeable discrepancies with the harmonic evolution of both trace gases, mainly during the latter years of the period considered. Oscillation was softer than observed with the harmonic equation for CO_2, and winter maxima were smaller for CH_4. However, weighted quadratic regression provided values close to those of the harmonic evolution.

Finally, the harmonic equation provided more regular changes and, in some way, proves less flexible than the other procedures that describe better the changes observed in relatively short times determining an irregular evolution.

4. Discussion

4.1. Observations

The CO_2 evolution presented in Fig. 1 is similar to that observed at different places. The lowest concentration was close to 400 ppm. Similar values were observed at Lin'an, China for the period 2009–2011 (Pu et al., 2014). However, Hernández-Paniagua et al. (2015) presented observations at southwest London where the lowest values were smaller, even reaching 350 ppm in the period 2000–2002. Similarly, the lowest values of CO_2 concentration at Cabaw, the Netherlands, were below 380 ppm (Vermeulen et al., 2011). The highest concentration at CIBA was occasionally above 500 ppm. Zhu and Yoshikawa-Inoue (2015) observed large episodic high CO_2 events during summer on Rishiri Island, western North Pacific, which were attributed to high emissions from local soil and vegetation and the stable nocturnal boundary layer. High values reached in spring at CIBA may have a similar origin, although some might be due to vehicles used in farming. The opposite behaviour was observed at Lin'an, where the highest values were more moderate. CH_4 measured at CIBA was confined at a narrow interval determined by the interquartile range, 0.040 ppm. Although the lowest values were similar to those observed at Cabaw, they were mainly located over a wider interval during the period 2000–2010.

4.2. Trend analysis

The range of trends presented in Table 1 is very wide since it extends 2.5 ppm $year^{-1}$. Wu et al. (2012) obtained the same value as that observed at CIBA, 1.7 ppm $year^{-1}$, which is close to the global average of the last decade, nearly 2.1 ppm $year^{-1}$ (WMO, 2016). This trend was similar in Mauna Loa, where it has been above 2.0 ppm $year^{-1}$ in recent years (Hofmann et al., 2009). The increase at the beginning of the measurement period was smaller than values presented in Table 1, whose lowest trend was 1.3 ppm $year^{-1}$ at a site in Antarctica. However, at the end of the measurement period the trend was similar to Egham, UK, or Pallas, Finland, although far from the highest, which was 3.8 ppm $year^{-1}$, observed in China.

Since interactions between natural and anthropogenic processes are complex, positive feedback in the biosphere determines the CO_2 increase. Among global scope processes, El Niño-Southern Oscillation is correlated with variations in the CO_2 growth rate (Heimann and Reichstein, 2008; Ruzmaikin et al., 2012). Moreover, different studies reveal that CO_2 uptake by terrestrial ecosystems (carbon sink) influences atmospheric CO_2 concentrations. Ahlström et al. (2015) concluded that semi-arid ecosystems dominate the trend and inter-annual variability of the sink. The role of winter snow in the northern forest merits further research since the decrease in winter respiration justifies the carbon sink enhancement (Yu et al., 2016). Additionally, observations over the last sixty years indicate that CO_2 uptake is stimulated during spring, while an earlier release of CO_2 into the atmosphere was observed in autumn

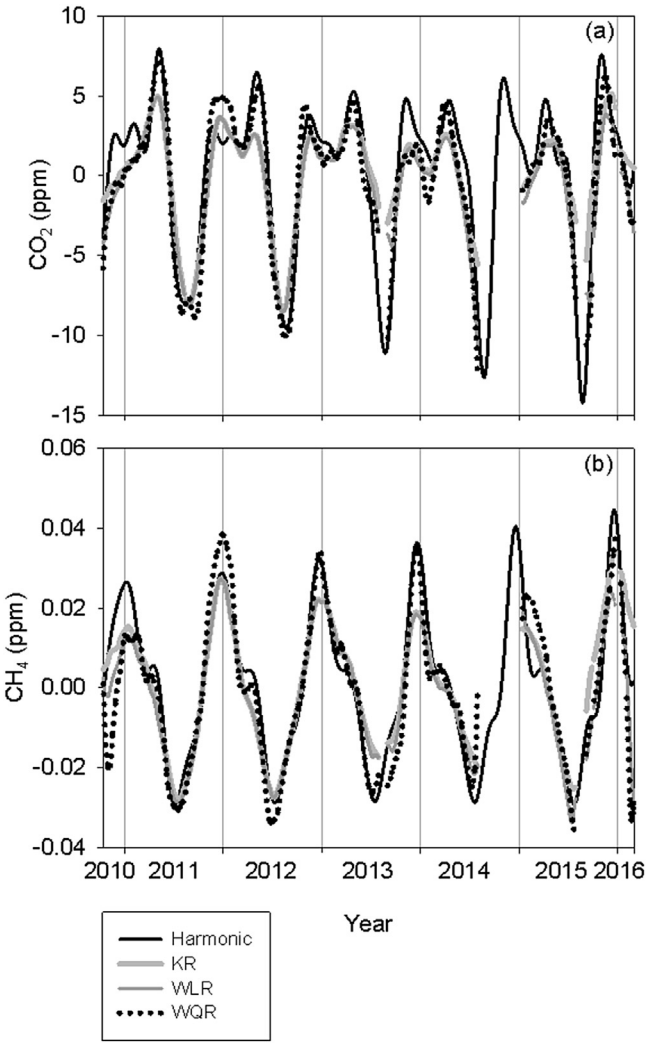

Fig. 5. Seasonal evolution of CO_2 (a) and CH_4 (b) for the harmonic equation, kernel regression (KR), weighted linear regression (WLR) and weighted quadratic regression (WQR).

(Sitch et al., 2015), and future studies should consider the effects of nonlinear interactions of dominant drivers on the trend of land carbon uptake (Zhang et al., 2016).

WMO (2016) presented growth rates for CH_4 in the range 0.005–0.010 ppm year^{-1} in recent years, which might partially be explained by the global impact of the increase in anthropogenic emissions in Asia (Dalsøren et al., 2016). Bergamaschi et al. (2013) described a growth rate peak of about 0.01 ppm year^{-1} in early 2007, preceded by a nearly null growth rate during 2005 and followed by slow attenuation. Vermeulen et al. (2011) provided a reference value of 0.0059 ppm year^{-1} for the period 2005–2010, which was similar to the value at CIBA, and a rate of 0.0074 ppm year^{-1} at Cabaw, the Netherlands (Table 2). The most noticeable trend presented in this table, about 0.050 ppm year^{-1}, was observed at Hegyhátsál, Hungary, although it corresponded to a short period, 2007–2009.

Increased emissions in the tropical and mid-latitude Northern Hemisphere are considered to be responsible for the CH_4 increase since 2007 (Nisbet et al., 2014), which may be explained by the increase in emissions from natural wetlands, fossil fuel-related emissions or the decrease in OH concentrations (Sussmann et al., 2012). Moreover, the current network does not allow a description of emissions by region and source processes and attributing this increase to natural and anthropogenic sources is not easy since emissions from both sources are superimposed (Bergamaschi et al., 2013). Additionally, the global scale of different processes should not be ignored. Ginzburg et al. (2011) considered the influence of the winter of 2006–2007, which was anomalously warm in northern Europe and western Siberia, on the CH_4 increase recorded in 2007. Similarly, anthropogenic emissions in Asia seem to have a global impact although their timing or strength has been questioned (Dalsøren et al., 2016).

4.3. Harmonic analysis

Sánchez et al. (2010) considered CO_2 evolution at CIBA from February 2000 to December 2008 by means of a simple harmonic model with two harmonics (for the yearly and half-yearly cycles), although only the yearly cycle presented variable amplitude. The half-yearly cycle was evident during the first years. However, the

Table 1
CO_2 trend and harmonic equations used in different studies.

Reference	Site	Trend (ppm year^{-1})	Period	Polynomial part	Harmonic part
Aalto et al. (2002)	Pallas, Finland	2.5	1996–2000	Linear	Three harmonics
Artuso et al. (2009)	Lampedusa, Italy	1.9	1992–2007		Two harmonics
Bakwin et al. (1998)	Eastern North Carolina		1992–1997	Second order	Four harmonics
	Northern Wisconsin		1994–1997		
Cundari et al. (1995)	Mt. Cimone, Italy	1.66	1979–1991		
Eneroth et al. (2005)	Pallas, Finland		1997–2003	Linear	Three harmonics
Fang et al. (2016)	Shangdianzi, China	2.7–3.8	2009–2013	Second order	Four harmonics
Hernández-Paniagua et al. (2015)	Egham, UK	2.45	2000–2012		
	Mace Head, Ireland	1.9	2000–2011		
Inoue et al. (2006)	Tsukuba, Japan	2.0	1992–2003	Fourth order	Three harmonics
Jain et al. (2005)	Maitri (Antarctica)	1.3	2002–2003		
Liu et al. (2015)	Different sites in the Northern Hemisphere	2.04	1997–2006	Linear	One harmonic
McClure et al. (2016)	Mt. Bachelor, Oregon	1.48	2012–2014		
Tans et al. (1989)	Point Barrow, Alaska	1.44	1983–1985	Linear	Four harmonics
Timokhina et al. (2015)	Central Siberia, Russia	2.02	2006–2013	Linear	Four harmonics
Vermeulen et al. (2011)	Cabaw, The Netherlands	2.00	2005–2009	Linear	Four harmonics
Wu et al. (2012)	Northeast China	1.7	2003–2010	Linear	One harmonic
Zhang et al. (2008)	Seven sites in China	1.7–3.6	2003–2006		

at latitudes above 45° N (Barichivich et al., 2013). Finally, uncertainties remain in the magnitude and sign of CO_2 sink trends

yearly cycle prevailed at the end. Yearly amplitude increased by 0.65 ppm year^{-1}. This value was similar to that provided by Eq. (3),

Table 2
CH_4 trend and harmonic equations used in different studies.

Reference	Site	Trend (ppm year^{-1})	Period	Polynomial part	Harmonic part
Fang et al. (2016)	Shangdianzi, China	0.006–0.010	2009–2013	Second order	Four harmonics
Haszpra et al. (2011)	Hegyhátsál, Hungary	0.050	2007–2009		
Nisbet et al. (2014)	Globally averaged	0.006	2007–2013		
Pedersen et al. (2005)	Mt. Zeppelin, Norway	0.00334–0.00363	1998–2005		
Vermeulen et al. (2011)	Cabaw, The Netherlands	0.0074	2005–2010	Linear	Four harmonics

which was 0.55 ppm year^{-1} for the lowest level.

Wu et al. (2012) considered only one harmonic with a variable amplitude to investigate CO_2 evolution in a tall forest in China, this reaching an increase in the seasonal cycle of 0.58 ppm year^{-1} and which was explained from measurements at Mauna Loa, Hawaii, by the biosphere's seasonal CO_2 "inhalations" and "exhalations" that have become more pronounced. Moreover, Arctic Oscillation led to an early spring and to higher winter temperatures, resulting in increased seasonal amplitudes.

Liu et al. (2015) presented CO_2 evolution over nine ecosystems in the period 1997–2006. They used only one harmonic with a variable amplitude. Concentrations seemed steady in three of them. Amplitude remained steady or increased slightly in four ecosystems, increasing clearly in three and decreasing in one. The amplitude in the last ecosystem first decreased, although it then increased after one very low value.

4.4. Seasonal cycle

The yearly behaviour for CO_2 described in Fig. 5 responds to the average seasonal cycle from WMO (2016). However, spring and autumn maxima are more marked in Fig. 5 since this plot corresponds to a specific site. Moreover, this figure is in agreement with that reported by Cundari et al. (1995), who presented the seasonal evolution in 1989 at Mt. Cimone, although the spring maximum was barely visible and a noticeable scatter of measurements was observed in summer. Such a cycle with two maxima was also described by Hatakka et al. (2003) for CO_2 concentration at Pallas, Finland, from 1997 to 2003.

Climate-vegetation-carbon cycle feedback is noticeable above 40° N. The seasonal CO_2 cycle has become more marked since the 1960s although the underlying mechanisms are not yet fully known (Forkel et al., 2016). The decreasing summer minima could be attributed to an increase in vegetation photosynthetic activity during the growing season (Angert et al., 2005). Similarly, Barichivich et al. (2013) concluded that the long term increase in the amplitude of the CO_2 annual cycle above 45° N over Eurasia is associated with the lengthening and intensification of the photosynthetic growing season.

A similar evolution to that observed for CH_4 at CIBA was reported by Pickers and Manning (2015) at the Alert Station in Canada and by Vermeulen et al. (2011) at Cabaw in the Netherlands where, in addition, a steady concentration was observed in spring. Although oxidation by OH contributes to the minimum obtained in summer, dispersive processes linked with the development of the boundary layer should not be ignored. Since observations of this variable are not available, the temperature at Valladolid, obtained from AEMET (2016), may be used instead. In winter, temperature is low and the boundary layer is barely developed, causing high concentration values. In summer, thermal turbulence was intense and produced well developed boundary layers, with low concentrations being observed. Temperature decrease from summer to winter is rapid. However, the temperature increase from winter to summer presents a period with steady values in spring, which may be linked to intermediate boundary layer heights and steady concentrations. However, in Waliguan, China, the annual pattern was the opposite, with one minimum in spring and winter and one maximum in summer. This specific evolution may be explained by regional and local sources together with the dominant airflow from polluted regions in summer (Zhang et al., 2013).

5. Conclusions

Amplitudes of the first and second harmonics are noticeable for CO_2, whereas only the first harmonic is enough for CH_4. These amplitudes present a linear evolution with time in the period October 2010–February 2016.

Trend calculation shows slight differences following the procedure used. Although the addition of polynomial and harmonic parts is common, alternative methods, such as kernel regression, may be successfully employed.

Trend increased for both trace gases with the different procedures used. However, seasonal analysis with the harmonic equation revealed an unequal trend for both gases, with minima decreasing for CO_2 and maxima increasing for CH_4. This behaviour may be because all observations are considered, whereas the rest of the methods used only local neighbouring observations when calculating.

Since small changes are observed not only in the trend but also in the yearly cycle of both trace gases, procedure selection should be guided by the simplicity of the formulation and by calculation speed. Taking into account these features, kernel regression provides fast and accurate values to determine the evolution of both trace gases for the trend and inside the yearly cycle.

Although the analysis presented in the current paper involved concentrations recorded at a semi-natural site, the influence of air mass trajectories on concentrations and their trends should be considered for a more accurate description of the evolution of both trace gases.

Conflict of interests

The authors declare that there is no conflict of interests regarding publication of this paper.

Acknowledgements

The authors wish to acknowledge the financial support of the Ministry of Economy and Competitiveness and ERDF funds (projects CGL2009-11979 and CGL2014-53948-P).

References

Aalto, T., Hatakka, J., Paatero, I., Tuovinen, J.P., Aurela, M., Laurila, T., Holmén, K., Trivett, N., Viisanen, Y., 2002. Tropospheric carbon dioxide concentrations at a northern boreal site in Finland: basic variations and source areas. Tellus, Ser. B Chem. Phys. Meteorol. 54, 110–126.

AEMET (Agencia Estatal de Meteorología), 2016. http://www.aemet.es/es/portada. Accessed, September 2016.

Ahlström, A., Raupach, M.R., Schurgers, G., Smith, B., Arneth, A., Jung, M., Reichstein, M., Canadell, J.G., Friedlingstein, P., Jain, A.K., Kato, E., Poulter, B., Sitch, S., Stocker, B.D., Viovy, N., Wang, Y.P., Wiltshire, A., Zaehle, S., Zeng, N.,

2015. The dominant role of semi-arid ecosystems in the trend and variability of the land CO_2 sink. Science 348, 895–899.
Angert, A., Biraud, S., Bonfils, C., Henning, C.C., Buermann, W., Pinzon, J., Tucker, C.J., Fung, I., 2005. Drier summers cancel out the CO_2 uptake enhancement induced by warmer springs. Proc. Natl. Acad. Sci. U. S. A. 102, 10823–10827.
Artuso, F., Chamard, P., Piacentino, S., Sferlazzo, D.M., De Silvestri, L., di Sarra, A., Meloni, D., Monteleone, F., 2009. Influence of transport and trends in atmospheric CO_2 at Lampedusa. Atmos. Environ. 43, 3044–3051.
Bakwin, P.S., Tans, P.P., Hurst, D.F., Zhao, C., 1998. Measurements of carbon dioxide on very tall towers: results of the NOAA/CMDL program. Tellus, Ser. B Chem. Phys. Meteorol. 50, 401–415.
Barichivich, J., Briffa, K.R., Myneni, R.B., Osborn, T.J., Melvin, T.M., Ciais, P., Piao, S., Tucker, C., 2013. Large-scale variations in the vegetation growing season and annual cycle of atmospheric CO_2 at high northern latitudes from 1950 to 2011. Glob. Change Biol. 19, 3167–3183.
Bergamaschi, P., Houweling, S., Segers, A., Krol, M., Frankenberg, C., Scheepmaker, R.A., Dlugokencky, E., Wofsy, S.C., Kort, E.A., Sweeney, C., Schuck, T., Brenninkmeijer, C., Chen, H., Beck, V., Gerbig, C., 2013. Atmospheric CH_4 in the first decade of the 21st century: inverse modeling analysis using SCIAMACHY satellite retrievals and NOAA surface measurements. J. Geophys. Res. D. Atmos. 118, 7350–7369.
Chamard, P., Thiery, F., Di Sarra, A., Ciattaglia, L., De Silvestri, L., Grigioni, P., Monteleone, F., Piacentino, S., 2003. Interannual variability of atmospheric CO_2 in the Mediterranean: measurements at the island of Lampedusa. Tellus, Ser. B Chem. Phys. Meteorol. 55, 83–93.
Chen, H., Winderlich, J., Gerbig, C., Hoefer, A., Rella, C.W., Crosson, E.R., Van Pelt, A.D., Steinbach, J., Kolle, O., Beck, V., Daube, B.C., Gottlieb, E.W., Chow, V.Y., Santoni, G.W., Wofsy, S.C., 2010. High-accuracy continuous airborne measurements of greenhouse gases (CO_2 and CH_4) using the cavity ring-down spectroscopy (CRDS) technique. Atmos. Meas. Tech. 3, 375–386.
Cleveland, R.B., Cleveland, W.S., McRae, J.E., Terpenning, I., 1990. STL: a seasonal-trend decomposition procedure based on loess. J. Off. Stat. 6, 3–73.
Cleveland, W.S., 1979. Robust locally weighted regression and smoothing scatterplots. J. Am. Stat. Assoc. 74, 829–836.
Cleveland, W.S., Devlin, S.J., 1988. Locally weighted regression: an approach to regression analysis by local fitting. J. Am. Stat. Assoc. 83, 596–610.
Crosson, E.R., 2008. A cavity ring-down analyzer for measuring atmospheric levels of methane, carbon dioxide, and water vapor. Appl. Phys. B 92, 403–408.
Cundari, V., Colombo, T., Ciattaglia, L., 1995. Thirteen years of atmospheric carbon dioxide measurements at Mt. Cimone station. Italy. Il Nuovo Cimento C 18, 33–47.
Dalsøren, S.B., Myhre, C.L., Myhre, G., Gomez-Pelaez, A.J., Søvde, O.A., Isaksen, I.S.A., Weiss, R.F., Harth, C.M., 2016. Atmospheric methane evolution the last 40 years. Atmos. Chem. Phys. 16, 3099–3126.
Donnelly, A., Misstear, B., Broderick, B., 2011. Application of nonparametric regression methods to study the relationship between NO_2 concentrations and local wind direction and speed at background sites. Sci. Total Environ. 409, 1134–1144.
Eneroth, K., Aalto, T., Hatakka, J., Holmén, K., Laurila, T., Viisanen, Y., 2005. Atmospheric transport of carbon dioxide to a baseline monitoring station in northern Finland. Tellus, Ser. B Chem. Phys. Meteorol. 57, 366–374.
Fang, S.X., Tans, P.P., Dong, F., Zhou, H., Luan, T., 2016. Characteristics of atmospheric CO_2 and CH_4 at the Shangdianzi regional background station in China. Atmos. Environ. 131, 1–8.
Forkel, M., Carvalhais, N., Rödenbeck, C., Keeling, R., Heimann, M., Thonicke, K., Zaehle, S., Reichstein, M., 2016. Enhanced seasonal CO_2 exchange caused by amplified plant productivity in northern ecosystems. Science 351, 696–699.
García, M.A., Sánchez, M.L., Pérez, I.A., Ozores, M.I., Pardo, N., 2016. Influence of atmospheric stability and transport on CH_4 concentrations in northern Spain. Sci. Total Environ. 550, 157–166.
Ginzburg, A.S., Vinogradova, A.A., Fedorova, E.I., 2011. Some features of seasonal variations in the methane content in the atmosphere over northern Eurasia. Izv. Atmos. Ocean. Phys. 47, 45–58.
Graven, H.D., Guilderson, T.P., Keeling, R.F., 2012. Observations of radiocarbon in CO_2 at La Jolla, California, USA 1992-2007: analysis of the long-term trend. J. Geophys. Res. D. Atmos. 117, D02302. http://dx.doi.org/10.1029/2011JD016533.
Haszpra, L., Barcza, Z., Szilágyi, I., Dlugokencky, E., Tans, P., 2011. Trends and temporal variations of major greenhouse gases at a rural site in central Europe. In: L. Haszpra (Ed.). Atmospheric Greenhouse Gases: the Hungarian Perspective, pp. 29–47.
Hatakka, J., Aalto, T., Aaltonen, V., Aurela, M., Hakola, H., Komppula, M., Laurila, T., Lihavainen, H., Paatero, J., Salminen, K., Viisanen, Y., 2003. Overview of the atmospheric research activities and results at Pallas GAW station. Boreal Environ. Res. 8, 365–383.
Heimann, M., Reichstein, M., 2008. Terrestrial ecosystem carbon dynamics and climate feedbacks. Nature 451, 289–292.
Henry, R.C., Chang, Y.S., Spiegelman, C.H., 2002. Locating nearby sources of air pollution by nonparametric regression of atmospheric concentrations on wind direction. Atmos. Environ. 36, 2237–2244.
Hernández-Paniagua, I.Y., Lowry, D., Clemitshaw, K.C., Fisher, R.E., France, J.L., Lanoisellé, M., Ramonet, M., Nisbet, E.G., 2015. Diurnal, seasonal, and annual trends in atmospheric CO_2 at southwest London during 2000-2012: wind sector analysis and comparison with Mace Head. Irel. Atmos. Environ. 105, 138–147.
Higuchi, K., Worthy, D., Chan, D., Shashkov, A., 2003. Regional source/sink impact on the diurnal, seasonal and inter-annual variations in atmospheric CO_2 at a boreal forest site in Canada. Tellus, Ser. B Chem. Phys. Meteorol. 55, 115–125.
Hofmann, D.J., Butler, J.H., Tans, P.P., 2009. A new look at atmospheric carbon dioxide. Atmos. Environ. 43, 2084–2086.
Inoue, H.Y., Matsueda, H., Igarashi, Y., Sawa, Y., Wada, A., Nemoto, K., Sartorius, H., Schlosser, C., 2006. Seasonal and long-term variations in atmospheric CO_2 and ^{85}Kr in Tsukuba, central Japan. J. Meteorol. Soc. Jpn. 84, 959–968.
Jacobson, M.Z., 2005. Erratum: "Control of fossil-fuel particulate black carbon and organic matter, possibly the most effective method of slowing global warming". J. Geophys. Res. D. Atmos. 110, 1–5.
Jain, S.L., Ghude, S.D., Kumar, A., Arya, B.C., Kulkarni, P.S., 2005. Continuous observations of surface air concentration of carbon dioxide and methane at Maitri. Antarct. Curr. Sci. 88, 1941–1948.
Liu, M., Wu, J., Zhu, X., He, H., Jia, W., Xiang, W., 2015. Evolution and variation of atmospheric carbon dioxide concentration over terrestrial ecosystems as derived from eddy covariance measurements. Atmos. Environ. 114, 75–82.
Lohila, A., Penttilä, T., Jortikka, S., Aalto, T., Anttila, P., Asmi, E., Aurela, M., Hatakka, J., Hellén, H., Henttonen, H., Hänninen, P., Kilkki, J., Kyllönen, K., Laurila, T., Lepistö, A., Lihavainen, H., Makkonen, U., Paatero, J., Rask, M., Sutinen, R., Tuovinen, J.P., Vuorenmaa, J., Viisanen, Y., 2015. Preface to the special issue on integrated research of atmosphere, ecosystems and environment at Pallas. Boreal Environ. Res. 20, 431–454.
McClure, C.D., Jaffe, D.A., Gao, H., 2016. Carbon dioxide in the free troposphere and boundary layer at the Mt. Bachelor observatory. Aerosol Air Qual. Res. 16, 717–728.
Nakazawa, T., Ishizawa, M., Higuchi, K., Trivett, N.B.A., 1997. Two curve fitting methods applied to CO_2 flask data. Environmetrics 8, 197–218.
Nisbet, E.G., Dlugokencky, E.J., Bousquet, P., 2014. Methane on the rise - again. Science 343, 493–495.
NOAA (National Oceanic and Atmospheric Administration, 2016. Global Monitoring Division. http://www.esrl.noaa.gov/gmd/. Accessed, September 2016.
Olivier, J.G.J., Janssens-Maenhout, G., Muntean, M., Peters, J.H.A.W., 2015. Trends in Global CO_2 Emissions - 2015 Report, JRC Report 98184/PBL Report 1803. http://edgar.jrc.ec.europa.eu/overview.php?v=CO2ts1990-2014. Accessed, September 2016.
Pedersen, I.T., Holmén, K., Hermansen, O., 2005. Atmospheric methane at zeppelin station in Ny-Ålesund: Presentation and analysis of in situ measurements. J. Environ. Monit. 7, 488–492.
Pickers, P.A., Manning, A.C., 2015. Investigating bias in the application of curve fitting programs to atmospheric time series. Atmos. Meas. Tech. 8, 1469–1489.
Pu, J.J., Xu, H.H., He, J., Fang, S.X., Zhou, L.X., 2014. Estimation of regional background concentration of CO_2 at Lin'an station in Yangtze river delta, China. Atmos. Environ. 94, 402–408.
Rella, C., 2010. Accurate Greenhouse Gas Measurements in Humid Gas Streams Using the Picarro G1301 Carbon Dioxide/Methane/Water Vapor Gas Analyzer. https://www.picarro.com/assets/docs/White_Paper_G1301_Water_Vapor_Correction.pdf. Accessed, June 2016.
Rella, C.W., Chen, H., Andrews, A.E., Filges, A., Gerbig, C., Hatakka, J., Karion, A., Miles, N.L., Richardson, S.J., Steinbacher, M., Sweeney, C., Wastine, B., Zellweger, C., 2013. High accuracy measurements of dry mole fractions of carbon dioxide and methane in humid air. Atmos. Meas. Tech. 6, 837–860.
Ruzmaikin, A., Aumann, H.H., Pagano, T.S., 2012. Patterns of CO_2 variability from global satellite data. J. Clim. 25, 6383–6393.
Sánchez, M.L., García, M.A., Pérez, I.A., Pardo, N., 2014. CH_4 continuous measurements in the upper Spanish plateau. Environ. Monit. Assess. 186, 2823–2834.
Sánchez, M.L., Pérez, I.A., García, M.A., 2010. Study of CO_2 variability at different temporal scales recorded in a rural Spanish site. Agric. For. Meterol 150, 1168–1173.
Sitch, S., Friedlingstein, P., Gruber, N., Jones, S.D., Murray-Tortarolo, G., Ahlström, A., Doney, S.C., Graven, H., Heinze, C., Huntingford, C., Levis, S., Levy, P.E., Lomas, M., Poulter, B., Viovy, N., Zaehle, S., Zeng, N., Arneth, A., Bonan, G., Bopp, L., Canadell, J.G., Chevallier, F., Ciais, P., Ellis, R., Gloor, M., Peylin, P., Piao, S.L., Le Quéré, C., Smith, B., Zhu, Z., Myneni, R., 2015. Recent trends and drivers of regional sources and sinks of carbon dioxide. Biogeosciences 12, 653–679.
Sussmann, R., Forster, F., Rettinger, M., Bousquet, P., 2012. Renewed methane increase for five years (2007-2011) observed by solar FTIR spectrometry. Atmos. Chem. Phys. 12, 4885–4891.
Tans, P.P., Thoning, K.W., Elliott, W.P., Conway, T.J., 1989. Background atmospheric CO_2 patterns from weekly flask samples at Barrow, Alaska: optimal signal recovery and error estimates. NOAA Tech. Mem. ERL ARL-173 112–123.
Thoning, K.W., Tans, P.P., 1989. Atmospheric carbon dioxide at Mauna Loa Observatory. 2. Analysis of the NOAA GMCC data, 1974-1985. J. Geophys. Res. 94, 8549–8565.
Timokhina, A.V., Prokushkin, A.S., Onuchin, A.A., Panov, A.V., Kofman, G.B., Verkhovets, S.V., Heimann, M., 2015. Long-term trend in CO_2 concentration in the surface atmosphere over Central Siberia. Russ. Meteorol. Hydrol. 40, 186–190.
Vermeulen, A.T., Hensen, A., Popa, M.E., Van Den Bulk, W.C.M., Jongejan, P.A.C., 2011. Greenhouse gas observations from Cabauw tall tower (1992-2010). Atmos. Meas. Tech. 4, 617–644.
Wada, A., Sawa, Y., Matsueda, H., Taguchi, S., Murayama, S., Okubo, S., Tsutsumi, Y., 2007. Influence of continental air mass transport on atmospheric CO_2 in the western North Pacific. J. Geophys. Res. D. Atmos. 112.
WDCGG (World Data Centre for Greenhouse Gases), 2016. http://ds.data.jma.go.jp/gmd/wdcgg/. Accessed, June 2016.
WMO, 2016. WDCGG No. 40, Japan Meteorological Agency. http://ds.data.jma.go.jp/

gmd/wdcgg/pub/products/summary/sum40/sum40contents.html. Accessed, June 2016.
Wu, J., Guan, D., Yuan, F., Yang, H., Wang, A., Jin, C., 2012. Evolution of atmospheric carbon dioxide concentration at different temporal scales recorded in a tall forest. Atmos. Environ. 61, 9–14.
Yu, Z., Wang, J., Liu, S., Piao, S., Ciais, P., Running, S.W., Poulter, B., Rentch, J.S., Sun, P., 2016. Decrease in winter respiration explains 25% of the annual northern forest carbon sink enhancement over the last 30 years. Glob. Ecol. Biogeogr. 25, 586–595.
Zhang, X., Rayner, P.J., Wang, Y.P., Silver, J.D., Lu, X., Pak, B., Zheng, X., 2016. Linear and nonlinear effects of dominant drivers on the trends in global and regional land carbon uptake: 1959 to 2013. Geophys. Res. Lett. 43, 1607–1614.
Zhang, F., Zhou, L.X., Xu, L., 2013. Temporal variation of atmospheric CH_4 and the potential source regions at Waliguan, China. Sci. China Earth Sci. 56, 727–736.
Zhang, D., Tang, J., Shi, G., Nakazawa, T., Aoki, S., Sugawara, S., Wen, M., Morimoto, S., Patra, P.K., Hayasaka, T., Saeki, T., 2008. Temporal and spatial variations of the atmospheric CO_2 concentration in China. Geophys. Res. Lett. 35.
Zhu, C., Yoshikawa-Inoue, H., 2015. Seven years of observational atmospheric CO_2 at a maritime site in northernmost Japan and its implications. Sci. Total Environ. 524–525, 331–337.